

Research Articles | Behavioral/Cognitive

Functional heterogeneity within the primate ventral striatum for motivational regulation

<https://doi.org/10.1523/JNEUROSCI.2430-24.2025>

Received: 23 December 2024

Revised: 2 April 2025

Accepted: 7 April 2025

Copyright © 2025 Iwaaki et al.

This is an open-access article distributed under the terms of the [Creative Commons Attribution 4.0 International license](#), which permits unrestricted use, distribution and reproduction in any medium provided that the original work is properly attributed.

This Early Release article has been peer reviewed and accepted, but has not been through the composition and copyediting processes. The final version may differ slightly in style or formatting and will contain links to any extended data.

Alerts: Sign up at www.jneurosci.org/alerts to receive customized email alerts when the fully formatted version of this article is published.

1 **Functional heterogeneity within the primate ventral striatum for**
2 **motivational regulation**

3 Abbreviated title: Motivational controls in monkey ventral striatum

4

5 Haruhiko Iwaoki¹, Yukiko Hori¹, Yuki Hori¹, Koki Mimura^{1,2}, Kei Oyama¹, Yuji Nagai¹,
6 Toshiyuki Hirabayashi¹, Ken-ichi Inoue³, Masahiko Takada³, Makoto Higuchi¹, and
7 Takafumi Minamimoto^{1*}

8

9 ¹Advanced Neuroimaging Center, National Institutes for Quantum Science and Technology,
10 Chiba, 263-8555, Japan

11 ²National Institute of Neuroscience, National Center of Neurology and Psychiatry, Tokyo,
12 187-8551, Japan

13 ³Systems Neuroscience Section, Center for the Evolutionary Origins of Human Behavior,
14 Kyoto University, Aichi, 484-8506, Japan

15

16 *Author to whom all correspondence should be addressed:

17 Takafumi Minamimoto, Ph.D.

18 Advanced Neuroimaging Center, National Institutes for Quantum Science and Technology.

19 4-9-1 Anagawa, Inage-ku, Chiba 263-8555, Japan

20 Email: minamimoto.takafumi@qst.go.jp

21

22 **Number of pages:** 33

23 **Number of figures:** 5, **supplemental tables:** 1

24 **Number of words for abstract:** 223 words, **introduction:** 650 words, **discussion:** 1511
25 words

26 **Conflict of interest statement:** The authors declare no competing financial interests.

27

28 **Acknowledgments**

29 This research was supported by MEXT/JSPS KAKENHI Grant Numbers JP20H05955 (to
30 TM), 24H00734 (to TH), 22H05157 (to KI), and JP23K12943 (to HI), by AMED Grant
31 JP24wm0625307 (to TH), and by JST ACT-X Grant Number JPMJAX24C4 (to HI). We
32 thank Erika Kikuchi, Jun Kamei, Yuichi Matsuda, Ryuji Yamaguchi, Yoshio Sugii, and Rie
33 Yoshida for their technical assistance.

JNeurosci Accepted Manuscript

34 Abstract

35 The ventral striatum (VS) is a key brain region for reward processing and motivation, and
36 its dysfunctions have been implicated in psychiatric disorders such as apathy and
37 obsessive-compulsive disorder. Although functional heterogeneity within the VS has been
38 well established in rodents, its relevance and mechanisms in primates remain unclear. To
39 address this issue, we performed bilateral pharmacological inactivation of the VS in two
40 male macaque monkeys using muscimol, a GABA_A receptor agonist. Precise targeting was
41 achieved through computed tomography and magnetic resonance imaging. Behavioral
42 effects were evaluated using two methods: a goal-directed task with variable rewards and
43 analysis of spontaneous behavior. Our results demonstrated that anterior (a)VS inactivation
44 induced a hypoactivity state that we termed “resting,” whereas posterior (p)VS inactivation
45 elicited compulsive-like “checking” behaviors. Notably, neither the aVS nor the pVS
46 inactivation affected reward value or drive processing, thus differentiating aVS and pVS
47 from those involved in incentive motivation, such as the rostromedial caudate and ventral
48 pallidum. Retrograde tracing demonstrated distinct anatomical projection patterns for the
49 aVS and pVS, supporting their functional segregation. Together, the present results
50 suggest the functional heterogeneity of the primate VS along its anterior–posterior axis,
51 with the aVS and pVS participating in distinct motivational control circuits. Our findings may
52 have important implications for understanding the neural mechanisms of psychiatric
53 disorders and for the development of new therapeutic approaches.

54

55 Significance Statement

56 The ventral striatum (VS) is a core brain region that is involved in motivation and reward-
57 based behaviors. Its dysfunction is implicated in psychiatric disorders such as apathy and
58 obsessive-compulsive disorder. In macaque monkeys, we used imaging-guided
59 pharmacological manipulations to reveal that the anterior and posterior VS subregions have
60 distinct roles in motivation, independent of the incentive or reward drive. Specifically,
61 anterior VS inactivation induced a hypoactive state, whereas posterior VS inactivation
62 elicited compulsive-like behaviors. These findings reveal distinct motivational mechanisms

63 within the primate VS, thus offering valuable insights into the neural basis of psychiatric
64 disorders and identifying promising therapeutic targets.

JNeurosci Accepted Manuscript

65 **Introduction**

66 Motivation is a psychological process that directs, initiates, and sustains behavior toward a
67 goal (Atkinson, 1964; Dickinson & Balleine, 1994). Disruptions in motivational control are
68 associated with various mental health disorders such as apathy where the initiation and
69 persistence of behaviors are impaired; obsessive-compulsive disorder (OCD) where
70 individuals become excessively motivated toward maladaptive behaviors (Figeo et al.,
71 2011; Gillan & Robbins, 2014; Levy & Dubois, 2006). Accordingly, an understanding of the
72 neural mechanisms of motivational control is critical from both biological and clinical
73 perspectives. This is especially important in nonhuman primates, whose brain anatomy,
74 function, and behavioral repertoire share significant similarities with those of humans.

75

76 The ventral striatum (VS) is a core part of the “reward circuit” and plays an important role in
77 motivational control because of its extensive anatomical connections with limbic cortical
78 and subcortical areas (Haber & Knutson, 2010; Haber & McFarland, 1999). In monkeys,
79 neuronal activity within the VS has been shown to signal various aspects of reward
80 processing, including magnitude, prediction, omission, timing of acquisition, and reward-
81 driven motivation (Bowman et al., 1996; Cromwell & Schultz, 2003; Hollerman et al., 1998;
82 Nakamura et al., 2012; Schultz et al., 1992; Shidara et al., 1998; Tremblay et al., 1998).
83 Complementary human neuroimaging studies have revealed that activity in the VS
84 correlates with both the amount of reward offered and the effort required to obtain a reward
85 (Knutson et al., 2001; Pessiglione et al., 2007). These findings suggest that the VS in
86 primates is crucial for both reward-related information processing and motivational control.

87

88 However, motivational control extends beyond reward-seeking behaviors, and growing
89 evidence suggests that the VS also regulates non-reward behaviors. In rodents, for
90 example, the optogenetic activation of neurons in the nucleus accumbens (a structure
91 within the VS) increases self-grooming behaviors (Zhang et al., 2021). In monkeys,
92 hypoactivity has been observed following the local activation of the VS (Worbe et al., 2009),
93 further suggesting that this region contributes to a broad range of motivational processes.

94 Moreover, experimental lesions of the primate VS do not directly impair reward behavior
95 (Stern & Passingham, 1996), and lesion-induced effects are limited compared to other
96 regions, such as the amygdala (Costa et al., 2016). These findings highlight serious
97 limitations to our current understanding of the specific roles of the primate VS in
98 motivational control.

99

100 Given the involvement of the VS in both spontaneous and reward-driven behaviors, the
101 behavioral consequences of VS manipulation need to be explored from multiple
102 perspectives. Specifically, regarding goal-directed behavior, classic psychological models
103 suggest that motivation is influenced by two factors: the incentive value of rewards and
104 drive (Hull, 1943; Spence, 1956; Toates, 1986). These factors should be evaluated
105 separately when studying how the VS governs goal-directed behaviors. In addition,
106 research in rodents has revealed that focal inactivation of the nucleus accumbens along its
107 anterior-posterior axis elicits opposing reactions, appetitive eating and defensive treading
108 (Reynolds & Berridge, 2001). However, the relatively deep location of the VS in the primate
109 brain poses challenges for identifying region-specific functions, which has resulted in a
110 substantial gap in our understanding of the VS functions between primates and rodents.

111

112 Here, we investigated the behavioral effects of VS inactivation in macaque monkeys
113 through the local injection of muscimol (a GABA_A receptor agonist) in both goal-directed
114 and free-moving behavioral contexts. For the goal-directed task, we used a motivational
115 paradigm that allowed us to distinguish the effects of incentive and drive on motivation for
116 action. Given that the limbic system generally exerts similar functions across both
117 hemispheres and lacks clear lateralization, unilateral manipulation may produce
118 compensatory effects. We therefore targeted mirror-symmetric regions of the VS precisely
119 under the guidance of computed tomography (CT) and magnetic resonance (MR) imaging.
120 Together with complementary anatomical tracing data, our findings revealed functional
121 differences within the primate VS in motivational control. These results suggest potential

122 implications for the underlying mechanisms of psychiatric conditions associated with

123 motivational dysregulation and offer novel approaches to their treatment.

124

JNeurosci Accepted Manuscript

125 **Materials and Methods**

126 *Subjects*

127 Three male rhesus monkeys (*Macaca mulatta*; monkey RI: 6.3 kg, monkey BI: 8.0 kg,
128 monkey #250: 6.1 kg) were used. Monkeys RI and BI were previously used in an
129 inactivation study targeting the rostromedial caudate nucleus and ventral pallidum
130 (Fujimoto et al., 2019; Nagai et al., 2016). All experimental procedures followed the Guide
131 for the Care and Use of Nonhuman Primates in Neuroscience Research (The Japan
132 Neuroscience Society; https://www.jnss.org/en/animal_primates) and were approved by the
133 Animal Ethics Committee of the National Institutes for Quantum Science and Technology
134 (#11-1038). Food was available ad libitum, and motivation was controlled by restricting
135 access to fluid before experimental sessions in which water was provided as a reward for
136 task performance. Animals received water supplementation whenever necessary (e.g.,
137 when they were unable to obtain sufficient water through experimentation) and had free
138 access to water whenever testing was interrupted for more than 1 week. For environmental
139 enrichment, play objects and/or small food items (fruit, nuts, and vegetables) were provided
140 daily in the home cages.

141

142 *Surgery*

143 Three monkeys underwent surgery under general isoflurane anesthesia (1%–2%) for the
144 implantation of either one or two chambers and a head fixation device (for monkeys BI and
145 RI) or before receiving a viral vector injection (for monkey #250) for the retrograde tracing
146 study (detailed below). For monkey BI, a single chamber (22 × 22 mm ID; KDS Ltd.) was
147 placed vertically, whereas for monkey RI, two chambers (19 mm ID; Crist Instrument Co.)
148 were placed at a 20° angle from the coronal plane. Prophylactic antibiotics and analgesics
149 were administered after surgery.

150

151 Prior to surgery, the stereotaxic coordinates of target brain structures were estimated using
152 overlaid MR and CT images created using PMOD image analysis software (PMOD
153 Technologies). The CT scans (Accuitomo170, J.Morita) and MR imaging (7 T,

154 NIRS/KOBELCO/Bruker or BioSpec 70/40, Bruker) were performed under anesthesia
155 (continuous intravenous infusion of propofol, 0.2–0.6 mg/kg/min, i.v.).

156

157 *Muscimol microinjection*

158 The GABA_A agonist muscimol (M1523, Sigma-Aldrich) was injected bilaterally and mirror-
159 symmetrically into the VS to inactivate neuronal activity, following previously reported
160 procedures (Nagai et al., 2016). Guide tubes were inserted through a grid hole in the
161 implanted injection chamber, and stainless steel cannulae (outer diameter 300 µm;
162 Muromachi Inc.) were advanced using a microdrive (MO-97A, Narishige Inc.). Muscimol (3
163 µg/1 µL saline) was injected at a rate of 0.2 µL/min using an auto-injector (Legato210, KD
164 Scientific Inc.) to simultaneously deliver a total volume of 2 µL per side. In the saline control
165 sessions, the same amount of saline was injected. The locations of injection cannulae were
166 visualized using CT scans before or after the behavioral tests, and tip locations were
167 mapped onto MR images using PMOD image analysis software (Fig. 1A). Saline control
168 injections and sham injections (guide tubes inserted without any injection) were used as
169 controls. The muscimol or control injections were performed once per week.

170

171 *Experimental design*

172 The behavioral effects of local VS inactivation were assessed in two contexts: spontaneous
173 behaviors in a test cage and goal-directed behaviors in a motivational task. Monkey RI
174 underwent either the free-moving test or the motivational task in a single experimental
175 session, with four exceptions (see Table S1). On the day of the free-moving test, a CT scan
176 was conducted to visualize the location of the injection cannulae (approximately 10 min),
177 followed by muscimol or saline injection (approximately 10 min). After a 30-min waiting
178 period, the monkey was placed in the test cage for 60 min of behavioral observations. On
179 the day of the motivational task, the task (approximately 100 min) was conducted after the
180 injection, followed by a CT scan. Monkey BI underwent both tests after all muscimol
181 injection sessions and in three control sessions in the following order: injection (10 min),
182 motivational task (100 min), CT scan (10 min), and free-moving test (60 min). The other

183 three control sessions were conducted similarly to those of monkey RI. The detailed
184 injection sites and experimental conditions are listed in Table S1.

185

186 *Spontaneous behaviors*

187 Spontaneous behaviors were assessed in an isolated test cage for 1 hour (Fig. 1B). For
188 monkey RI, the test cage was its home cage, which was located out of sight of other
189 monkeys. Monkey BI was tested in a room with no other monkeys present. Monkey
190 behavior was recorded at 30 frames per second using a video camera (RealSense D435,
191 Intel) positioned in front of the cage. Monkeys were habituated to the recording
192 environment for 2–3 weeks prior to testing. During recording, the water bottle and feeding
193 box were removed, and the cage was illuminated using light-emitting diode (LED) lights.

194

195 *Goal-directed behavior*

196 Each monkey was seated in a primate chair in a sound-attenuated dark room for the
197 behavioral training and testing. Visual stimuli were presented on a computer video monitor
198 placed in front of the monkey. Behavioral control data and data acquisition were performed
199 using a real-time experimentation system (REX) (Hays et al., 1982), and visual stimuli were
200 displayed using Presentation software (Neurobehavioral Systems). In the reward-size task
201 (Fig. 1C), the monkey had to release a bar to obtain liquid rewards. Trials began when the
202 monkey touched the bar at the front of the chair. After a visual cue and a red target (the
203 wait signal) appeared on the monitor, the target turned green following a variable interval
204 (0.5–1.5 s). The monkey then had to release the bar between 0.2 and 1 s to receive a liquid
205 reward (1–8 drops of water, 1 drop = approximately 0.12 mL). In each trial, the visual cues
206 were randomly changed. An inter-trial interval of 1 s was enforced before the next trial
207 began. If the monkey released the bar before the green target appeared, released the bar
208 within 0.2 s after it appeared (early release), or failed to release the bar within 1 s (late
209 release), the trial was terminated immediately and was repeated after the 1-s inter-trial
210 interval. Before each testing session, monkeys were subject to approximately 22 hours of
211 water restriction without any behavioral testing. Each testing session continued for 100 min.

212

213 *Statistical analysis*

214 In the free-moving context, spontaneous behaviors were categorized into the five most
215 observed behaviors: “standing” (standing up on two legs), “resting” (sitting with head down
216 and motionless), “grooming” (self-grooming), “checking” (manipulating the corners of the
217 cage with fingertips), and “biting” (biting the chain of the collar). To quantify these
218 behaviors, we implemented an object detection deep learning algorithm (You Only Look
219 Once [YOLO] v5; <https://github.com/ultralytics/yolov5>) to analyze postural patterns in the
220 video recordings on a frame-by-frame basis. To minimize redundancy and enhance
221 generalizability, 100 representative frames were extracted from each session using a k-
222 means frame selection method implemented in DeepLabCut 2.1 (Mathis et al., 2018). An
223 expert experimenter familiar with monkey behaviors manually annotated each frame by
224 drawing a bounding box around the monkey and labeling it with one of the five behavioral
225 categories when applicable. Separate YOLO models were trained for each monkey using
226 80% of the annotated frames for training and 20% for testing. The models achieved mean
227 average precision scores of 0.87 for monkey RI and 0.84 for monkey BI. These trained
228 models were then applied to automatically classify behaviors across all video frames in
229 each session. For each session, the number of frames classified into each behavioral
230 category was counted, and the relative proportion of each behavior was calculated. For
231 data-driven clustering based on the five characteristic behaviors, Ward’s hierarchical
232 clustering method (Ward, 1963) with Euclidean distance was applied to the behavioral data
233 (maximum number of clusters = 10). To statistically assess the regional differences in the
234 expression of “checking” and “resting” behaviors, chi-square tests were conducted
235 separately for each monkey.

236

237 For the reward-size task, error rates in task performance were calculated by dividing the
238 total number of errors by the total number of trials for each reward size, and were then
239 averaged across all sessions. Error rates were fitted to an inverse function of reward size,
240 $E = 1/aR$, where R is the reward size, a is a constant parameter for all individual subjects,
241 and E is the error rate (%) of the monkeys in trials with reward size R . The details were as

242 follows (as reported in Minamimoto et al., 2009). We performed repeated measures
243 analysis of variance (ANOVA) with subjects as a random effect to examine the effect of
244 treatment x reward size on error rate as well as the effect of treatment on the total number
245 of errors and trials, rewards earned, and average reaction times in each session. Post-hoc
246 comparisons were made using Tukey's honestly significant difference test, with statistical
247 significance = 0.05. The data of rostromedial caudate and ventral pallidum inactivation
248 were reanalyzed from data originally obtained by Nagai et al. (2016) and Fujimoto et al.
249 (2019), respectively.

250

251 *Retrograde tracing study*

252 In monkey #250, retrograde tracing was performed using adeno-associated virus 2-retro
253 (AAV2retro) vectors expressing fluorescent proteins. Injections targeted the anterior (a)VS
254 (AAV2retro-hSyn-mScarlet) and posterior (p)VS (AAV2retro-hSyn-AcGFP). The AAV titer
255 was 2.0×10^{13} particles/mL and the volume was 1 μ L. The injections were performed with
256 the assistance of the Brainsight Vet Robot System (VRCT002, Rogue Research). The
257 intraoperative localization of injection cannulae was navigated using Brainsight (Rogue
258 Research) based on overlaid images of preoperative MRI and CT data. The vectors were
259 pressure-injected using a 10- μ L syringe (Model 1701RN, Hamilton) with a 30-gauge
260 injection needle placed in a fused silica capillary (outer diameter 450 μ m), which minimized
261 backflow by creating a 500-nm space surrounding the needle tip. The microsyringe was
262 mounted into a motorized microinjector (UMP3T-2, WPI) that was held by the robot arm.
263 After a burr hole (8 mm in diameter) and a hole in the dura mater (approximately 5 mm in
264 diameter) were made, the injection needle was inserted into the brain and slowly moved
265 down to 2 mm beyond the target. It was maintained stationary for 5 min before being pulled
266 up to the target location. The injection speed was set at 0.25 μ L/min. After the injection, the
267 needle remained in situ for 15 min to minimize backflow along the needle. Additional
268 surgical procedures are outlined in the *Surgery* section.

269

270 *Histology and image acquisition*

271 Following a survival period of 34 days, monkey #250 was immobilized using ketamine (10
272 mg/kg, intramuscular) and xylazine (0.5 mg/kg, intramuscular), deeply anesthetized with an
273 overdose of sodium thiopental (50 mg/kg, intravenous), and then transcardially perfused
274 with saline at 4°C followed by 4% paraformaldehyde in 0.1 M phosphate-buffered saline
275 (pH 7.4). The brain was removed from the skull, postfixed in the same fresh fixative
276 overnight, and saturated with 30% sucrose in phosphate buffer at 4°C. Coronal sections
277 (50 µm) were then cut serially using a freezing microtome. For double immunofluorescence
278 to detect green fluorescent protein (GFP) and red fluorescent protein (RFP), the sections
279 were blocked in 1% skim milk at room temperature for 1 hour. They were then incubated
280 for 2 days at 4°C in a mixture of rabbit anti-GFP monoclonal antibody (1:1,000 dilution;
281 Invitrogen) and rat anti-RFP monoclonal antibody (1:1,000 dilution; Proteintech) in 0.1 M
282 phosphate-buffered saline containing 2% normal donkey serum and 0.1% Triton X-100.
283 The sections were subsequently incubated for 2 hours at room temperature with a cocktail
284 of Alexa 488-conjugated donkey anti-rabbit IgG antibody (1:400 dilution; Thermo Fisher
285 Scientific) and Alexa 555-conjugated donkey anti-rat IgG antibody (1:400 dilution; Thermo
286 Fisher Scientific). Images of the stained sections were then captured using a digital slide
287 scanner (Nano-Zoomer S60, Hamamatsu Photonics K.K.; 20× objective, 0.46 µm per pixel)
288 or a microscope equipped with a high-grade charge-coupled device camera (Biorevo,
289 Keyence). The images were imported into a personal computer as digital data, and
290 fluorescent protein expression was confirmed by enlarging the images. The locations of
291 labeled neurons were plotted onto a macaque atlas (Dubach & Bowden, 2009; Rohlfing et
292 al., 2012, <https://scalablebrainatlas.incf.org/macaque/DB09>) for the anatomical analysis.

293

294 **Results**

295 We locally inactivated the bilateral VS by injecting muscimol, a GABA_A receptor agonist,
296 across 29 sessions in two monkeys (6 and 23 sessions for monkeys BI and RI,
297 respectively). We examined changes in spontaneous behavior in 13 muscimol sessions (6
298 and 7 sessions for monkeys BI and RI, respectively) and compared them with those in 10
299 control sessions (3 and 7 sessions, respectively). We also examined behavioral changes in
300 a goal-directed task during 26 muscimol sessions (6 and 20 sessions for monkeys BI and
301 RI, respectively) and compared them with those in 16 control sessions (6 and 10 sessions,
302 respectively). The details of the injection conditions and locations are summarized in Table
303 S1 and illustrated in Figure 1A.

304

305 ***Effects of VS inactivation on spontaneous behaviors***

306 To examine the effects of VS inactivation on spontaneous behaviors, we isolated each
307 monkey in its cage for 1 hour to minimize social interactions (Fig. 1B). The monkeys
308 showed five characteristic behaviors during the experiment. In control sessions, the
309 predominant behaviors were “standing” and “grooming” for both monkeys. However, VS
310 inactivation induced two atypical behaviors in both monkeys: “resting” and “checking.”

311

312 “Resting” was characterized by the monkeys sitting motionless with their head down, but
313 not lying down (Fig. 2A, top). By contrast, “checking” involved repetitive pinching at the
314 corners of the cage, accompanied by a series of varied movements and postural changes
315 such as sitting and standing (Fig. 2A, bottom). This behavior differed from simple
316 movement deficits such as motor tics. Notably, “checking” may have been accompanied by
317 negative emotions because the monkeys also displayed threatening behaviors toward other
318 monkeys upon returning to their home cages. Moreover, these inactivation-induced
319 behaviors of “resting” and “checking” were absent when the experimenter was present or
320 visible, such as during transfer to the test cage.

321

322 To link the injection sites with spontaneous behaviors, we analyzed video recordings using
323 a deep learning algorithm (YOLO; see *Materials and Methods*). Following inactivation of
324 anterior VS, “resting” was predominantly observed (Fig. 2A, purple bars). By contrast,
325 “checking” appeared more frequently after inactivation of posterior VS (Fig. 2A, red bars).
326 These site-dependent effects on behavior were consistent between sessions and monkeys,
327 and showed a clear distinction from those in control sessions (Fig. 2B). Although monkey
328 BI occasionally displayed postures resembling “resting” in control sessions, these were
329 often accompanied by grooming or other behaviors and clearly differed from sustained
330 “resting” observed during anterior VS inactivation sessions. A data-driven clustering
331 analysis further validated these site-specific behavioral effects, identifying five behavioral
332 clusters (Fig. 2C). Clusters 1 and 5, representing resting- and checking-dominant sessions,
333 respectively, corresponded exclusively to muscimol sessions (Fig. 2C, bottom). The other
334 three clusters consisted mainly of control sessions, with two exceptions: the sessions of
335 muscimol injections into the most anterior and posterior sites in monkey RI (mus-R7 and
336 mus-R1), which were categorized into clusters 3 and 4, respectively. The injection sites
337 corresponding to cluster 1 were located in the anterior VS (0–4 mm from the anterior tip;
338 Fig. 2D, cyan), whereas those for cluster 5 were located in the posterior VS (4–6 mm from
339 the anterior tip; Fig. 2D, magenta). The functional heterogeneity of proportions of “resting”
340 and “checking” behaviors emerged along the anterior–posterior axis of the primate VS with
341 a clear boundary (4 mm from the anterior tip; VS +4mm), which cannot be explained by
342 chance in either monkey (chi-squared test, $\chi^2(1) > 161,096$, $p < 1.0 \times 10^{-16}$). These results
343 indicate a significant site-dependent inactivation effect on spontaneous behaviors and thus
344 refer to these two regions as the aVS and pVS.

345

346 ***Effects of VS inactivation on goal-directed behaviors***

347 To examine the effects of local VS inactivation on goal-directed behaviors, we tested the
348 monkeys using the reward-size task (Fig. 1C). In this task, the monkeys released a bar
349 within 1 s after the color change of the fixation point to obtain a liquid reward (1, 2, 4, or 8
350 drops), which was cued at the beginning of each trial. If they released the bar incorrectly—
351 either too early (early errors) or too late (late errors)—the same stimulus–reward pair was

352 repeated in the subsequent trial, without the option to skip any undesired reward
353 conditions.

354

355 Similar to the effects observed in the free-moving context, VS inactivation in the goal-
356 directed context induced site-specific atypical behaviors (“resting” or “checking”) and
357 interfered with task performance. In control sessions, monkeys typically released the bar
358 with minimal hand movements. However, after pVS inactivation, superfluous hand
359 movements unrelated to the task sequence were made, leading to increased overall errors.
360 By contrast, aVS inactivation caused the monkeys to close their eyes and cease performing
361 the task for several to tens of minutes.

362

363 We analyzed the temporal dynamics of these atypical behaviors and their relationship with
364 reward accumulation over time. At the beginning of the aVS inactivation sessions, errors
365 progressively increased; this pattern was similar to that of the control sessions (Fig. 3A,
366 blue and black, respectively) and to the typical patterns observed in normal monkeys
367 (Minamimoto et al., 2009). Approximately 30 min later, however, the monkeys started to
368 intermittently rest and stop performing the task; this slowed their rate of reward
369 accumulation (Fig. 3B, blue) and led to significantly fewer total rewards earned compared
370 with those in the control sessions (one-way ANOVA, $F_{(2,39)} = 14.6$, $p = 1.97 \times 10^{-5}$; post-
371 hoc, aVS vs. control, $p = 0.044$, pVS vs. control, $p = 2.8 \times 10^{-4}$). Nonetheless, the monkeys
372 occasionally resumed the task and performed it correctly, indicating that they did not
373 abandon the task entirely.

374

375 In contrast to aVS injection, pVS injection caused a rapid increase in error trials at
376 approximately 30 min after the beginning of the session (Fig. 3A, red), resulting in a
377 significantly higher total number of errors compared with those in the control sessions (one-
378 way ANOVA, $F_{(2,39)} = 122.6$, $p = 2.0 \times 10^{-6}$; post-hoc, $p = 1.22 \times 10^{-13}$). Despite inefficient
379 task performance, the monkeys continued to engage in the task, albeit with slower
380 accumulation of rewards in the later part of the session. Consequently, their total rewards

381 remained significantly lower than those of controls (Fig. 3B, red; post-hoc, pVS vs. control,
382 $p = 2.8 \times 10^{-4}$). Together, these results suggest that reward drive was preserved even with
383 VS inactivation, because the monkeys did not completely abandon the task.

384

385 These site-dependent profiles of VS inactivation were further validated; inactivation of aVS,
386 but not pVS, significantly reduced the total number of trials initiated (Fig. 3C; one-way
387 ANOVA, $F_{(2,39)} = 7.804$, $p = 0.0015$; post-hoc, aVS vs. control, $p = 0.041$, pVS vs. control, p
388 $= 0.32$). Conversely, pVS inactivation increased the number of premature responses, as
389 indicated by a significantly increased ratio of early errors (Fig. 3D; one-way ANOVA, $F_{(2,39)}$
390 $= 92.12$, $p = 2.67 \times 10^{-15}$; post-hoc, $p = 1.33 \times 10^{-13}$). The observed anterior–posterior
391 differences in total errors (Fig. 3E) further emphasized the dichotomy of the inactivation
392 effects.

393

394 When the pVS was inactivated unilaterally (left VS +5.25 mm in monkey BI), the
395 characteristic “checking” behavior observed during bilateral inactivation was absent in the
396 free-moving context. Similarly, in the goal-directed task, unilateral inactivation did not result
397 in the significant increase in errors that was typically observed in the latter part of the
398 session. Although a higher early error rate (51.1%) was noted in unilateral pVS inactivation
399 compared with control conditions, this effect did not substantially disrupt overall
400 performance because the cumulative error count remained relatively low (unilateral pVS:
401 188 errors, bilateral pVS: 721 ± 90.2 errors; mean \pm standard error of the mean). These
402 findings suggest that the behavioral changes described earlier, including “checking” and
403 increased error rates, likely require bilateral VS inhibition to fully manifest.

404

405 ***Effects of VS inactivation and drive shift***

406 Given the significant effects of VS inactivation on goal-directed behavior, we sought to
407 determine whether these effects stemmed from altered motivation or from changes in
408 specific components of motivation, such as incentives or drive. Notably, we observed that
409 behavioral effects became prominent approximately 30 min after the session onset,

410 regardless of the location of VS inactivation. This timing suggests that the emergence of
411 behavioral changes might be related to a shift in the internal drive state because thirst
412 presumably decreased with reward accumulation. To explore this idea, we analyzed error
413 rates during the first and last 25 min of each session, representing the high- and low-drive
414 states, respectively (Fig. 4A and 4B).

415

416 In the first 25 min of aVS inactivation sessions, error rates remained low and were
417 comparable with those of controls (two-way ANOVA, main effect of treatment, $F_{(1, 112)} =$
418 0.01 , $p = 0.94$). There was also a significant main effect of reward size, with an inverse
419 relationship between reward size and errors (Fig. 4A, bottom left; $F_{(3, 112)} = 10.56$, $p =$
420 0.042), consistent with the findings of previous studies using this task (Fujimoto et al.,
421 2019; Hori et al., 2021; Minamimoto et al., 2009; Nagai et al., 2016). In the last 25 min, the
422 overall error rate increased for both control and aVS inactivation sessions—likely reflecting
423 reduced thirst-driven motivation—but no main effect of treatment or interaction was
424 observed, although the effect of reward size remained significant (Fig. 4A, bottom right;
425 treatment, $F_{(1, 112)} = 0.01$, $p = 0.94$; reward size, $F_{(3, 112)} = 12.02$, $p = 0.035$; treatment \times
426 reward size, $F_{(3, 112)} = 0.99$, $p = 0.504$). These results suggest that aVS inactivation does
427 not disturb motivational processing for goal-directed behaviors.

428

429 Similarly, pVS inactivation did not alter the error pattern in the first 25 min (Fig. 4B, bottom
430 left; treatment, $F_{(1, 112)} = 3.098$, $p = 0.33$; reward size, $F_{(3, 112)} = 10.09$, $p = 0.045$; treatment
431 \times reward size, $F_{(3, 112)} = 7.78$, $p = 0.063$). However, in the last 25 min, the error rates
432 drastically increased specifically in pVS sessions regardless of reward size, resulting in a
433 significant main effect of treatment (Fig. 4B, bottom right; two-way ANOVA, treatment, $F_{(1,$
434 $112)} = 212$, $p = 0.044$; reward size, $F_{(3, 112)} = 8.82$, $p = 0.054$; treatment \times reward size, $F_{(3, 112)}$
435 $= 2.8$, $p = 0.21$). These results suggest that, although motivational processing initially
436 remained intact following pVS inactivation, a progressive disruption of motivational control
437 occurred as reflected by increased errors over time.

438

439 The temporal dynamics observed in the present study suggest that the delayed onset of
440 task-relevant behavior likely reflects a shift in each monkey's internal drive. Early in the
441 task, when thirst drive dominated, competing drives such as resting or exploration were
442 suppressed, allowing for goal-directed behavior. As thirst diminished, these competing
443 drives became more prominent, leading to the emergence of task-irrelevant behaviors.
444 However, an alternative explanation involves muscimol pharmacodynamics; it may be that
445 the initial effects of muscimol are too mild to immediately disrupt task performance.

446

447 To address the possible mechanisms underlying the above findings more closely, we
448 conducted additional muscimol injections in regions adjacent to the aVS and pVS: the
449 rostromedial caudate (rmCD), located dorsally to the aVS (Fig. 4C top), and the ventral
450 pallidum (VP), located 2–4 mm caudally to the pVS (Fig. 4D top). rmCD inactivation
451 produced significantly higher error rates within the initial 25 min compared with controls
452 (Fig. 4C, bottom left; two-way ANOVA, treatment, $F_{(1, 199)} = 8.47$, $p = 0.004$; reward size, $F_{(3, 199)} = 3.013$, $p = 0.0312$). In the last 25 min, error rates further increased, and a significant
453 interaction between reward size and treatment emerged (Fig. 4C, bottom right; two-way
454 ANOVA, treatment, $F_{(1, 199)} = 31.05$, $p = 3.12 \times 10^{-8}$; reward size, $F_{(3, 199)} = 7.51$, $p = 8.75 \times$
455 10^{-5} ; treatment \times reward size, $F_{(3, 199)} = 5.0$, $p = 0.0023$). Similarly, VP inactivation produced
456 significant effects in both the initial and final 25 min, in which the main effect of reward size
457 disappeared and a significant main effect of treatment emerged (two-way ANOVA, first 25
458 min, treatment, $F_{(1, 71)} = 46.28$, $p = 2.69 \times 10^{-9}$, reward size, $F_{(3, 71)} = 0.35$, $p = 0.79$; last 25
459 min, treatment, $F_{(1, 71)} = 1212.51$, $p = 2.28 \times 10^{-46}$, reward size, $F_{(3, 71)} = 2.55$, $p = 0.063$).

460 These results indicate that muscimol injections can induce behavioral changes immediately
461 after the session onset, suggesting that the delayed effects observed with aVS and pVS
462 inactivation are unlikely to be caused by muscimol kinetics or spatial diffusion.

463

464 Together, these results support the idea that the delayed emergence of task-irrelevant
465 behaviors following aVS and pVS inactivation likely arose because of a diminished thirst
466 drive, thus allowing other desires (such as rest and exploration) to become more influential.
467

468 Furthermore, the marked impact of rmCD and VP inactivation on motivational value—
469 specifically, the altered relationship between reward size and error rate—emphasizes the
470 importance of these regions in incentive processing. This finding contrasts with the effects
471 observed with VS inactivation, and underscores the unique roles of the VS in both
472 processing multiple drives and regulating behaviors according to the balance among these
473 drives.

474

475 Finally, we examined the effects of VS inactivation on other behavioral indices. There was
476 no significant treatment effect on reaction time for either the first or last 25 min (Fig. 4B;
477 two-way ANOVA, first 25 min, treatment, $F_{(2, 168)} = 10.68$, $p = 0.086$, reward size, $F_{(3, 168)} =$
478 14.96 , $p = 0.026$; last 25 min, treatment, $F_{(2, 168)} = 0.21$, $p = 0.83$, reward size, $F_{(3, 168)} =$
479 7.67 , $p = 0.064$). These results further suggest that the VS does not play a direct role in the
480 initiation of goal-directed action.

481

482 ***Distinct cortical and subcortical inputs to the aVS and pVS revealed by retrograde*** 483 ***tracing***

484 The finding that aVS and pVS inactivation induced different atypical behaviors with a clear
485 functional boundary between these regions suggests that each region is a part of distinct
486 neural circuits that differentially controls behavior. To investigate this concept, we
487 performed a retrograde tracer study to map the cortical and subcortical connections that
488 are specific to the aVS and pVS regions. AAV2retro-hSyn-mScarlet and -AcGFP vectors
489 were injected into the left aVS (VS +3 mm) and right pVS (VS +5 mm), respectively, in an
490 additional monkey (monkey #250). The injection sites were confirmed by observing
491 localized fluorescent signals within the intended regions, without any overlap along the
492 anterior–posterior axis; however, we noted minor leakage into the caudate nucleus, which
493 is dorsal to the aVS (Fig. 5A).

494

495 The retrogradely labeled neurons of the aVS (red) and pVS (green) were mapped onto a
496 macaque atlas (Fig. 5B). Both regions commonly received projections from the medial
497 prefrontal cortex, including its ventral part (areas 10mc, 14c, 14r, and 32), and the
498 entorhinal cortex (Fig. 5B-1 to -3). By contrast, in the aVS only, labeled neurons were also
499 identified in the anterior insular cortex and temporal cortex (Fig. 5B-4, Left). In addition,
500 retrogradely labeled neurons of the pVS were selectively observed in the lateral
501 orbitofrontal cortex (area 11l), dorsomedial prefrontal cortex (areas 8Bm and 9m), and
502 dorsal anterior cingulate cortex (area 24c; Fig. 5B-1 to -3, Right), as well as in the basal
503 nucleus and accessory basal nucleus of the amygdala (Fig. 5B-4, Right).

504

505 In terms of anterograde projections, axon terminals from both the aVS and pVS were
506 labeled in several brain regions, including the ventral pallidum, ventral tegmental area, and
507 internal segment of the globus pallidus. Visual inspection of fluorescence labeling revealed
508 no clear differences in projection patterns between the aVS and pVS in these brain regions,
509 suggesting that some output pathways may be shared between the two VS regions.

510

511 These anatomical results support the hypothesis that the aVS and pVS form distinct neural
512 circuits, especially in terms of their origins of projection. The “resting” behavior induced by
513 aVS inactivation may be controlled by regions uniquely connected to the aVS, such as the
514 anterior insula, whereas the “checking” behavior induced by pVS inactivation may be
515 mediated by regions specifically connected to the pVS, including the lateral orbitofrontal
516 cortex and amygdala. This distinct connectivity between the aVS and pVS aligns with the
517 functional heterogeneity observed between the two regions, thus highlighting their
518 specialized roles in motivational and behavioral regulation.

519 **Discussion**

520 In the present study, we examined the effects of inactivating mirror-symmetrical VS regions
521 on free-moving and goal-directed behaviors in macaque monkeys. We revealed that the
522 primate VS is functionally heterogeneous, comprising distinct aVS and pVS regions.
523 Inactivating these regions resulted in two specific behaviors: “resting” and “checking.”
524 “Resting” was characterized by a low-activation state, whereas “checking” resembled
525 stereotyped, compulsive-like behaviors rather than a motor disorder. These behaviors were
526 not observed during unilateral inactivation, suggesting that bilaterality is crucial for the
527 manifestation of these region-specific effects. Notably, despite these behavioral changes,
528 VS inactivation did not affect incentive processes or reward drives in goal-directed tasks.
529 Furthermore, retrograde tracing experiments demonstrated that the aVS and pVS have
530 distinct neural connections, indicating that these regions form separate cortico-striatal
531 circuits. Our findings suggest that the aVS and pVS are critical for regulating intrinsic
532 drives, thus orienting the organism toward appropriate/impending behaviors. The
533 inactivation of each region appears to elicit specific behavioral repertoires, reflecting their
534 functional specialization.

535

536 The primate VS is generally considered to be associated with motivational control,
537 particularly in terms of reward-driven behaviors; numerous electrophysiological and
538 neuroimaging studies emphasize the neural correlates of the VS in reward expectation and
539 rewarding events (Botvinick et al., 2009; Bowman et al., 1996; Cromwell & Schultz, 2003;
540 Croxson et al., 2009; Hollerman et al., 1998; Knutson et al., 2001; Knutson et al., 2005;
541 Knutson et al., 2000; Nakamura et al., 2012; Schultz et al., 1992; Shidara et al., 1998;
542 Tremblay et al., 1998). However, primate lesion studies suggest that the VS may not be a
543 center for reward-driven behavior (Stern & Passingham, 1996; Costa et al., 2016). This
544 ongoing debate led us to further explore its functions, specifically investigating potential
545 functional differentiation along the anterior–posterior axis, similar to findings in rodents
546 (Reynolds & Berridge, 2001, 2002, 2008).

547

548 In our study, we used CT and MR imaging to precisely inject muscimol into bilateral and
549 symmetrical regions of the VS while minimizing the effects on nearby reward-related brain
550 regions. We examined the causal role of the VS under two different motivational conditions.
551 Using a task that allowed us to separate two motivational factors—incentive value and
552 reward drive—we demonstrated that VS inactivation led to the emergence of non-reward-
553 dependent atypical behaviors such as “resting” and “checking” without impairing incentive
554 value or reward drive in the goal-directed task. This suggests that the VS may not regulate
555 goal-directed behavior solely based on reward value or internal drive, but may instead play
556 a critical role in controlling and suppressing various motivation types. VS inactivation
557 appeared to release these superfluous behaviors, which interfered with goal-directed
558 activity.

559

560 In free-moving contexts, monkeys showed atypical behaviors (“resting” or “checking”)
561 throughout the entire session. However, in goal-directed tasks, these behaviors only
562 emerged after 30 min, raising questions about the underlying mechanisms. Our
563 comparative analysis of previous data from the inactivation of VS-adjacent regions, the
564 rmCD and VP (Fujimoto et al., 2019; Nagai et al., 2016), clearly indicated that the effects
565 appeared immediately after task initiation. This suggests that the delayed appearance of
566 atypical behaviors following VS inactivation is unlikely to be caused by a slow
567 pharmacological onset. Instead, it is more likely that an initially high reward drive
568 suppresses other competing drives such as rest, which become prominent after the reward
569 drive diminishes. This temporal pattern contrasts with the directly impaired incentive-based
570 behaviors from task initiation with rmCD and VP inactivation. These findings suggest that
571 while the rmCD and VP are directly involved in incentive motivation, the VS may play a
572 broader regulatory role by suppressing competing, non-reward-driven motivations.

573

574 One limitation of our study is the potential spread of muscimol beyond the intended regions
575 of the VS. Although the potential effects on nearby regions cannot be completely ignored
576 when estimating the spread of muscimol (2–3 mm in diameter for a 2- μ L)(Murata et al.,

577 2015; Tremblay et al., 2009), they remained within the VS in most of the injections (see Fig.
578 1A, 2D, and 3E). Furthermore, the distinct and consistent behaviors that we observed,
579 which were clearly associated with locations along the VS anterior–posterior axis, suggest
580 that muscimol spread was likely confined to the target regions. The absence of any
581 intermediate or mixed behaviors at the aVS/pVS border further supports this conclusion.

582

583 The series of studies on rodent nucleus accumbens conducted by Berridge and colleagues
584 offer important insights into the functions of the VS in primates (Baumgartner et al., 2020;
585 Castro & Berridge, 2014; Reynolds & Berridge, 2001, 2002; Richard et al., 2013). These
586 earlier studies demonstrated that muscimol inactivation of the rostral and caudal regions of
587 the nucleus accumbens medial shell produces opposing motivational behaviors—appetitive
588 eating and defensive treading for the rostral and caudal shell, respectively. Although these
589 positive and negative motivational behaviors are different from the “resting” and “checking”
590 behaviors observed in our study, they may reflect species-specific differences in the
591 expression of motivational states.

592

593 The neuropsychological mechanisms driving the atypical behaviors induced by aVS and
594 pVS inactivation remain key to interpreting our findings. The “resting” behavior observed
595 after aVS inactivation resembles sleep in that monkeys became motionless. However,
596 typical sleep behaviors, such as lying down, were not noted, and monkeys only rested
597 when the experimenter was absent; this suggests a more voluntary, controlled resting state
598 rather than homeostatic sleep. This behavior is reminiscent of hypoactivity with preserved
599 executive function, as observed with unilateral pharmacological activation of the monkey
600 VS (Worbe et al., 2009).

601

602 By contrast, the “checking” behavior induced by pVS inactivation involved repetitive actions
603 that were distinct from motor disturbances such as tics. This behavior was akin to
604 compulsive grooming in rodents, which is elicited by the activation of excitatory inputs to
605 the VS from the orbitofrontal cortex and midbrain dopamine neurons (Ahmari et al., 2013;

606 Xue et al., 2022). Comparable behaviors have been reported in primates following the
607 manipulation of specific brain regions (Grabli et al., 2004; Rotge et al., 2012; Saga et al.,
608 2022; Worbe et al., 2009). The repetitive nature of “checking” may also serve as a new
609 model of OCD in humans. Although compulsive behaviors in clinical settings vary, ranging
610 from washing and cleaning to checking, the “checking” behaviors observed in the present
611 study represent a form of stereotyped behavior that has not previously been reported, and
612 may offer new insights into the neural mechanisms of OCD.

613

614 The concept of a “security motivation system,” proposed by Szechman and Woody (2004),
615 may explain the neuropsychological basis of compulsive-like behaviors observed in this
616 study. According to this model, behaviors such as checking are driven by an inability to
617 achieve a “feeling of knowing” that the environment is secure, leading to compulsive
618 behavior. The pVS may be a central component of such a security motivation system, and
619 its impairment might explain the emergence of compulsive-like behaviors.

620

621 Our anatomical tracing study suggests that while the VS projection patterns were largely
622 consistent with previous findings (Chikama et al., 1997; Fudge et al., 2004; Fudge & Haber,
623 2002; Fudge et al., 2002; Fudge & Tucker, 2009; Gimenez-Amaya et al., 1995; Haber et
624 al., 2000; Haber et al., 2006; Haber et al., 1995; Haber, Lynd, et al., 1990; Haber, Wolfe, et
625 al., 1990), aVS and pVS form distinct cortico-subcortical circuits. This adds finer granularity
626 to previously reported anterior–posterior distinctions in cortico-limbic striatal projections,
627 particularly those contrasting the VS with more posterior limbic regions such as the caudate
628 tail (McHale et al., 2022). These distinctions provide potential insights into conditions such
629 as apathy and OCD, as observed in the phenomenological similarities between the
630 behaviors induced by VS inactivation and these symptoms. The low-activity “resting” state
631 induced by aVS inactivation may be related to symptoms of apathy, particularly the “auto-
632 activation deficit” described in human patients (Levy & Dubois, 2006). Interestingly, the
633 insular cortex, which sends selective projection outputs to the aVS, reportedly shows
634 atrophy in patients with apathy (Moon et al., 2014). Moreover, the “checking” behavior
635 observed with pVS inactivation mirrors the compulsive behaviors commonly seen in OCD.

636 Human imaging studies of OCD patients have revealed activation in the lateral orbitofrontal
637 cortex and amygdala (Rotge et al., 2010; Simon et al., 2010), both of which send selective
638 outputs to the pVS. Notably, clinical studies have reported that the targets of deep brain
639 stimulation (DBS) for treatment-resistant OCD patients shifted to posterior regions of VS
640 (Greenberg et al., 2010). These behavioral circuit parallels suggest that further elucidation
641 of the neural mechanisms centered on the aVS and pVS may enhance our understanding
642 of the underlying mechanisms of clinical conditions, such as apathy and OCD, and might
643 lead to the identification of effective treatment targets.

644

645 In conclusion, the present study demonstrates that the aVS and pVS play distinct roles in
646 regulating non-reward-dependent behaviors, such as “resting” or “checking,” which emerge
647 following region-specific inactivation. Our findings suggest that the VS not only governs
648 reward-driven actions but also suppresses competing motivations, thereby underscoring its
649 broader role in behavioral regulation. The similarities between these behaviors and the
650 symptoms observed in apathy and OCD suggest the existence of similar underlying neural
651 mechanisms, thus offering new insights into potential therapeutic targets for psychiatric
652 conditions.

653 **References**

- 654 Ahmari, S. E., Spellman, T., Douglass, N. L., Kheirbek, M. A., Simpson, H. B., Deisseroth,
 655 K., Gordon, J. A., & Hen, R. (2013). Repeated cortico-striatal stimulation generates
 656 persistent OCD-like behavior. *Science*, *340*(6137), 1234-1239.
 657 <https://doi.org/10.1126/science.1234733>
- 658 Atkinson, J. W. (1964). *An introduction to motivation*. [https://psycnet.apa.org/record/1964-](https://psycnet.apa.org/record/1964-35038-000)
 659 [35038-000](https://psycnet.apa.org/record/1964-35038-000)
- 660 Baumgartner, H. M., Cole, S. L., Olney, J. J., & Berridge, K. C. (2020). Desire or Dread
 661 from Nucleus Accumbens Inhibitions: Reversed by Same-Site Optogenetic
 662 Excitations. *J Neurosci*, *40*(13), 2737-2752.
 663 <https://doi.org/10.1523/JNEUROSCI.2902-19.2020>
- 664 Botvinick, M. M., Huffstetler, S., & McGuire, J. T. (2009). Effort discounting in human
 665 nucleus accumbens. *Cogn Affect Behav Neurosci*, *9*(1), 16-27.
 666 <https://doi.org/10.3758/CABN.9.1.16>
- 667 Bowman, E. M., Aigner, T. G., & Richmond, B. J. (1996). Neural signals in the monkey
 668 ventral striatum related to motivation for juice and cocaine rewards. *J Neurophysiol*,
 669 *75*(3), 1061-1073. <https://doi.org/10.1152/jn.1996.75.3.1061>
- 670 Castro, D. C., & Berridge, K. C. (2014). Opioid hedonic hotspot in nucleus accumbens
 671 shell: mu, delta, and kappa maps for enhancement of sweetness "liking" and
 672 "wanting". *J Neurosci*, *34*(12), 4239-4250.
 673 <https://doi.org/10.1523/JNEUROSCI.4458-13.2014>
- 674 Chikama, M., McFarland, N. R., Amaral, D. G., & Haber, S. N. (1997). Insular cortical
 675 projections to functional regions of the striatum correlate with cortical
 676 cytoarchitectonic organization in the primate. *J Neurosci*, *17*(24), 9686-9705.
 677 <https://doi.org/10.1523/JNEUROSCI.17-24-09686.1997>
- 678 Costa, V. D., Dal Monte, O., Lucas, D. R., Murray, E. A., & Averbeck, B. B. (2016).
 679 Amygdala and Ventral Striatum Make Distinct Contributions to Reinforcement
 680 Learning. *Neuron*, *92*(2), 505-517. <https://doi.org/10.1016/j.neuron.2016.09.025>

- 681 Cromwell, H. C., & Schultz, W. (2003). Effects of expectations for different reward
 682 magnitudes on neuronal activity in primate striatum. *J Neurophysiol*, 89(5), 2823-
 683 2838. <https://doi.org/10.1152/jn.01014.2002>
- 684 Croxson, P. L., Walton, M. E., O'Reilly, J. X., Behrens, T. E., & Rushworth, M. F. (2009).
 685 Effort-based cost-benefit valuation and the human brain. *J Neurosci*, 29(14), 4531-
 686 4541. <https://doi.org/10.1523/JNEUROSCI.4515-08.2009>
- 687 Dickinson, A., & Balleine, B. (1994). Motivational Control of Goal-Directed Action. *Animal*
 688 *Learning & Behavior*, 22(1), 1-18. [https://doi.org/Doi 10.3758/Bf03199951](https://doi.org/Doi%2010.3758/Bf03199951)
- 689 Dubach M.F., & Bowden D.M. (2009). BrainInfo online 3D macaque brain atlas: a database
 690 in the shape of a brain. Society for Neuroscience Annual Meeting, Chicago, IL
 691 Abstract No. 199.5. <https://scalablebrainatlas.incf.org/macaque/DB09>
- 692 Figeo, M., Vink, M., de Geus, F., Vulink, N., Veltman, D. J., Westenberg, H., & Denys, D.
 693 (2011). Dysfunctional reward circuitry in obsessive-compulsive disorder. *Biol*
 694 *Psychiatry*, 69(9), 867-874. <https://doi.org/10.1016/j.biopsych.2010.12.003>
- 695 Fudge, J. L., Breitbart, M. A., & McClain, C. (2004). Amygdaloid inputs define a caudal
 696 component of the ventral striatum in primates. *J Comp Neurol*, 476(4), 330-347.
 697 <https://doi.org/10.1002/cne.20228>
- 698 Fudge, J. L., & Haber, S. N. (2002). Defining the caudal ventral striatum in primates:
 699 cellular and histochemical features. *J Neurosci*, 22(23), 10078-10082.
 700 <https://doi.org/10.1523/JNEUROSCI.22-23-10078.2002>
- 701 Fudge, J. L., Kunishio, K., Walsh, P., Richard, C., & Haber, S. N. (2002). Amygdaloid
 702 projections to ventromedial striatal subterritories in the primate. *Neuroscience*,
 703 110(2), 257-275. [https://doi.org/10.1016/s0306-4522\(01\)00546-2](https://doi.org/10.1016/s0306-4522(01)00546-2)
- 704 Fudge, J. L., & Tucker, T. (2009). Amygdala projections to central amygdaloid nucleus
 705 subdivisions and transition zones in the primate. *Neuroscience*, 159(2), 819-841.
 706 <https://doi.org/10.1016/j.neuroscience.2009.01.013>
- 707 Fujimoto, A., Hori, Y., Nagai, Y., Kikuchi, E., Oyama, K., Suhara, T., & Minamimoto, T.
 708 (2019). Signaling Incentive and Drive in the Primate Ventral Pallidum for

- 709 Motivational Control of Goal-Directed Action. *J Neurosci*, 39(10), 1793-1804.
710 <https://doi.org/10.1523/JNEUROSCI.2399-18.2018>
- 711 Gillan, C. M., & Robbins, T. W. (2014). Goal-directed learning and obsessive-compulsive
712 disorder. *Philos Trans R Soc Lond B Biol Sci*, 369(1655).
713 <https://doi.org/10.1098/rstb.2013.0475>
- 714 Gimenez-Amaya, J. M., McFarland, N. R., de las Heras, S., & Haber, S. N. (1995).
715 Organization of thalamic projections to the ventral striatum in the primate. *J Comp*
716 *Neurol*, 354(1), 127-149. <https://doi.org/10.1002/cne.903540109>
- 717 Grabli, D., McCairn, K., Hirsch, E. C., Agid, Y., Feger, J., Francois, C., & Tremblay, L.
718 (2004). Behavioural disorders induced by external globus pallidus dysfunction in
719 primates: I. Behavioural study. *Brain*, 127(Pt 9), 2039-2054.
720 <https://doi.org/10.1093/brain/awh220>
- 721 Greenberg, B. D., Gabriels, L. A., Malone, D. A., Jr., Rezai, A. R., Friehs, G. M., Okun, M.
722 S., Shapira, N. A., Foote, K. D., Cosyns, P. R., Kubu, C. S., Malloy, P. F., Salloway,
723 S. P., Gftakis, J. E., Rise, M. T., Machado, A. G., Baker, K. B., Stypulkowski, P. H.,
724 Goodman, W. K., Rasmussen, S. A., & Nuttin, B. J. (2010). Deep brain stimulation
725 of the ventral internal capsule/ventral striatum for obsessive-compulsive disorder:
726 worldwide experience. *Mol Psychiatry*, 15(1), 64-79.
727 <https://doi.org/10.1038/mp.2008.55>
- 728 Haber, S. N., Fudge, J. L., & McFarland, N. R. (2000). Striatonigrostriatal pathways in
729 primates form an ascending spiral from the shell to the dorsolateral striatum. *J*
730 *Neurosci*, 20(6), 2369-2382. [https://doi.org/10.1523/JNEUROSCI.20-06-](https://doi.org/10.1523/JNEUROSCI.20-06-02369.2000)
731 [02369.2000](https://doi.org/10.1523/JNEUROSCI.20-06-02369.2000)
- 732 Haber, S. N., Kim, K. S., Maily, P., & Calzavara, R. (2006). Reward-related cortical inputs
733 define a large striatal region in primates that interface with associative cortical
734 connections, providing a substrate for incentive-based learning. *J Neurosci*, 26(32),
735 8368-8376. <https://doi.org/10.1523/JNEUROSCI.0271-06.2006>

- 736 Haber, S. N., & Knutson, B. (2010). The reward circuit: linking primate anatomy and human
737 imaging. *Neuropsychopharmacology*, 35(1), 4-26.
738 <https://doi.org/10.1038/npp.2009.129>
- 739 Haber, S. N., Kunishio, K., Mizobuchi, M., & Lynd-Balta, E. (1995). The orbital and medial
740 prefrontal circuit through the primate basal ganglia. *J Neurosci*, 15(7 Pt 1), 4851-
741 4867. <https://doi.org/10.1523/JNEUROSCI.15-07-04851.1995>
- 742 Haber, S. N., Lynd, E., Klein, C., & Groenewegen, H. J. (1990). Topographic organization
743 of the ventral striatal efferent projections in the rhesus monkey: an anterograde
744 tracing study. *J Comp Neurol*, 293(2), 282-298.
745 <https://doi.org/10.1002/cne.902930210>
- 746 Haber, S. N., & McFarland, N. R. (1999). The concept of the ventral striatum in nonhuman
747 primates. *Ann N Y Acad Sci*, 877, 33-48. [https://doi.org/10.1111/j.1749-
748 6632.1999.tb09259.x](https://doi.org/10.1111/j.1749-6632.1999.tb09259.x)
- 749 Haber, S. N., Wolfe, D. P., & Groenewegen, H. J. (1990). The relationship between ventral
750 striatal efferent fibers and the distribution of peptide-positive woolly fibers in the
751 forebrain of the rhesus monkey. *Neuroscience*, 39(2), 323-338.
752 [https://doi.org/10.1016/0306-4522\(90\)90271-5](https://doi.org/10.1016/0306-4522(90)90271-5)
- 753 Hays, A. V., Richmond, B. J., & Optican, L. M. (1982). A UNIX-based multiple-process
754 system for real-time data acquisition and control. *WESCON Conf Proc* 2:1-10.
- 755 Hollerman, J. R., Tremblay, L., & Schultz, W. (1998). Influence of reward expectation on
756 behavior-related neuronal activity in primate striatum. *J Neurophysiol*, 80(2), 947-
757 963. <https://doi.org/10.1152/jn.1998.80.2.947>
- 758 Hori, Y., Nagai, Y., Mimura, K., Suhara, T., Higuchi, M., Bouret, S., & Minamimoto, T.
759 (2021). D1- and D2-like receptors differentially mediate the effects of dopaminergic
760 transmission on cost-benefit evaluation and motivation in monkeys. *PLoS Biol*,
761 19(7), e3001055. <https://doi.org/10.1371/journal.pbio.3001055>
- 762 Hull, C. L. (1943). *Principles of behavior: an introduction to behavior theory*.

- 763 Knutson, B., Adams, C. M., Fong, G. W., & Hommer, D. (2001). Anticipation of increasing
764 monetary reward selectively recruits nucleus accumbens. *J Neurosci*, *21*(16),
765 RC159. <https://doi.org/10.1523/JNEUROSCI.21-16-j0002.2001>
- 766 Knutson, B., Taylor, J., Kaufman, M., Peterson, R., & Glover, G. (2005). Distributed neural
767 representation of expected value. *J Neurosci*, *25*(19), 4806-4812.
768 <https://doi.org/10.1523/JNEUROSCI.0642-05.2005>
- 769 Knutson, B., Westdorp, A., Kaiser, E., & Hommer, D. (2000). fMRI visualization of brain
770 activity during a monetary incentive delay task. *Neuroimage*, *12*(1), 20-27.
771 <https://doi.org/10.1006/nimg.2000.0593>
- 772 Levy, R., & Dubois, B. (2006). Apathy and the functional anatomy of the prefrontal cortex-
773 basal ganglia circuits. *Cereb Cortex*, *16*(7), 916-928.
774 <https://doi.org/10.1093/cercor/bhj043>
- 775 McHale, A. C., Cho, Y. T., & Fudge, J. L. (2022). Cortical Granularity Shapes the
776 Organization of Afferent Paths to the Amygdala and Its Striatal Targets in
777 Nonhuman Primate. *J Neurosci*, *42*(8), 1436-1453.
778 <https://doi.org/10.1523/JNEUROSCI.0970-21.2021>
- 779 Mathis, A., Mamidanna, P., Cury, K. M., Abe, T., Murthy, V. N., Mathis, M. W., & Bethge, M.
780 (2018). DeepLabCut: Markerless pose estimation of user-defined body parts with
781 deep learning. *Nat Neurosci*, *21*(9), 1281-1289. [https://doi.org/10.1038/s41593-018-](https://doi.org/10.1038/s41593-018-0209-y)
782 [0209-y](https://doi.org/10.1038/s41593-018-0209-y)
- 783 Minamimoto, T., La Camera, G., & Richmond, B. J. (2009). Measuring and modeling the
784 interaction among reward size, delay to reward, and satiation level on motivation in
785 monkeys. *J Neurophysiol*, *101*(1), 437-447. <https://doi.org/10.1152/jn.90959.2008>
- 786 Moon, Y., Moon, W. J., Kim, H., & Han, S. H. (2014). Regional atrophy of the insular cortex
787 is associated with neuropsychiatric symptoms in Alzheimer's disease patients. *Eur*
788 *Neurol*, *71*(5-6), 223-229. <https://doi.org/10.1159/000356343>
- 789 Murata, Y., Higo, N., Hayashi, T., Nishimura, Y., Sugiyama, Y., Oishi, T., Tsukada, H., Isa,
790 T., & Onoe, H. (2015). Temporal plasticity involved in recovery from manual

- 791 dexterity deficit after motor cortex lesion in macaque monkeys. *J Neurosci*, 35(1),
792 84-95. <https://doi.org/10.1523/JNEUROSCI.1737-14.2015>
- 793 Nagai, Y., Kikuchi, E., Lerchner, W., Inoue, K. I., Ji, B., Eldridge, M. A., Kaneko, H., Kimura,
794 Y., Oh-Nishi, A., Hori, Y., Kato, Y., Hirabayashi, T., Fujimoto, A., Kumata, K.,
795 Zhang, M. R., Aoki, I., Suhara, T., Higuchi, M., Takada, M., . . . Minamimoto, T.
796 (2016). PET imaging-guided chemogenetic silencing reveals a critical role of
797 primate rostromedial caudate in reward evaluation. *Nat Commun*, 7, 13605.
798 <https://doi.org/10.1038/ncomms13605>
- 799 Nakamura, K., Santos, G. S., Matsuzaki, R., & Nakahara, H. (2012). Differential reward
800 coding in the subdivisions of the primate caudate during an oculomotor task. *J*
801 *Neurosci*, 32(45), 15963-15982. <https://doi.org/10.1523/JNEUROSCI.1518-12.2012>
- 802 Pessiglione, M., Schmidt, L., Draganski, B., Kalisch, R., Lau, H., Dolan, R. J., & Frith, C. D.
803 (2007). How the brain translates money into force: a neuroimaging study of
804 subliminal motivation. *Science*, 316(5826), 904-906.
805 <https://doi.org/10.1126/science.1140459>
- 806 Reynolds, S. M., & Berridge, K. C. (2001). Fear and feeding in the nucleus accumbens
807 shell: rostrocaudal segregation of GABA-elicited defensive behavior versus eating
808 behavior. *J Neurosci*, 21(9), 3261-3270. [https://doi.org/10.1523/JNEUROSCI.21-](https://doi.org/10.1523/JNEUROSCI.21-09-03261.2001)
809 [09-03261.2001](https://doi.org/10.1523/JNEUROSCI.21-09-03261.2001)
- 810 Reynolds, S. M., & Berridge, K. C. (2002). Positive and negative motivation in nucleus
811 accumbens shell: bivalent rostrocaudal gradients for GABA-elicited eating, taste
812 "liking"/"disliking" reactions, place preference/avoidance, and fear. *J Neurosci*,
813 22(16), 7308-7320. <https://doi.org/10.1523/JNEUROSCI.22-16-07308.2002>
- 814 Reynolds, S. M., & Berridge, K. C. (2008). Emotional environments retune the valence of
815 appetitive versus fearful functions in nucleus accumbens. *Nat Neurosci*, 11(4), 423-
816 425. <https://doi.org/10.1038/nn2061>
- 817 Richard, J. M., Castro, D. C., Difeliceantonio, A. G., Robinson, M. J., & Berridge, K. C.
818 (2013). Mapping brain circuits of reward and motivation: in the footsteps of Ann

- 819 Kelley. *Neurosci Biobehav Rev*, 37(9 Pt A), 1919-1931.
820 <https://doi.org/10.1016/j.neubiorev.2012.12.008>
- 821 Rohlfing T, Kroenke CD, Sullivan EV, Dubach MF, Bowden DM, Grant KA, Pfefferbaum A
822 (2012) "The INIA19 Template and NeuroMaps Atlas for Primate Brain Image
823 Parcellation and Spatial Normalization." *Frontiers in Neuroinformatics* 6:27.
824 <http://dx.doi.org/10.3389/fninf.2012.00027>
- 825 Rotge, J. Y., Aouizerate, B., Amestoy, V., Lambrecq, V., Langbour, N., Nguyen, T. H.,
826 Dovero, S., Cardoit, L., Tignol, J., Bioulac, B., Burbaud, P., & Guehl, D. (2012). The
827 associative and limbic thalamus in the pathophysiology of obsessive-compulsive
828 disorder: an experimental study in the monkey. *Transl Psychiatry*, 2(9), e161.
829 <https://doi.org/10.1038/tp.2012.88>
- 830 Rotge, J. Y., Langbour, N., Jaafari, N., Guehl, D., Bioulac, B., Aouizerate, B., Allard, M., &
831 Burbaud, P. (2010). Anatomical alterations and symptom-related functional activity
832 in obsessive-compulsive disorder are correlated in the lateral orbitofrontal cortex.
833 *Biol Psychiatry*, 67(7), e37-38. <https://doi.org/10.1016/j.biopsych.2009.10.007>
- 834 Saga, Y., Galineau, L., & Tremblay, L. (2022). Impulsive and compulsive behaviors can be
835 induced by opposite GABAergic dysfunctions inside the primate ventral pallidum.
836 *Front Syst Neurosci*, 16, 1009626. <https://doi.org/10.3389/fnsys.2022.1009626>
- 837 Schultz, W., Apicella, P., Scarnati, E., & Ljungberg, T. (1992). Neuronal activity in monkey
838 ventral striatum related to the expectation of reward. *J Neurosci*, 12(12), 4595-
839 4610. <https://doi.org/10.1523/JNEUROSCI.12-12-04595.1992>
- 840 Shidara, M., Aigner, T. G., & Richmond, B. J. (1998). Neuronal signals in the monkey
841 ventral striatum related to progress through a predictable series of trials. *J*
842 *Neurosci*, 18(7), 2613-2625. [https://doi.org/10.1523/JNEUROSCI.18-07-](https://doi.org/10.1523/JNEUROSCI.18-07-02613.1998)
843 [02613.1998](https://doi.org/10.1523/JNEUROSCI.18-07-02613.1998)
- 844 Simon, D., Kaufmann, C., Musch, K., Kischkel, E., & Kathmann, N. (2010). Fronto-striato-
845 limbic hyperactivation in obsessive-compulsive disorder during individually tailored

- 846 symptom provocation. *Psychophysiology*, 47(4), 728-738.
847 <https://doi.org/10.1111/j.1469-8986.2010.00980.x>
- 848 Spence, K. W. (1956). *Behavior theory and conditioning*. <https://doi.org/10.1037/10029-000>
- 849 Stern, C. E., & Passingham, R. E. (1996). The nucleus accumbens in monkeys (*Macaca*
850 *fascicularis*): II. Emotion and motivation. *Behav Brain Res*, 75(1-2), 179-193.
851 [https://doi.org/10.1016/0166-4328\(96\)00169-6](https://doi.org/10.1016/0166-4328(96)00169-6)
- 852 Szechtman, H. & Woody, E. (2004). Obsessive-compulsive disorder as a disturbance of
853 security motivation. *Psychological Review*, 111(1), 111-127.
854 <https://doi.org/10.1037/0033-295x.111.1.111>
- 855 Toates, F. M. (1986). *Motivational Systems*.
- 856 Tremblay, L., Hollerman, J. R., & Schultz, W. (1998). Modifications of reward expectation-
857 related neuronal activity during learning in primate striatum. *J Neurophysiol*, 80(2),
858 964-977. <https://doi.org/10.1152/jn.1998.80.2.964>
- 859 Tremblay, L., Worbe, Y., & Hollerman, J. R. (2009). *The ventral striatum: a heterogeneous*
860 *structure involved in reward processing, motivation, and decision-making*.
861 <https://doi.org/https://doi.org/10.1016/B978-0-12-374620-7.00003-0>
- 862 Ward, J. H. (1963). Hierarchical Grouping to Optimize an Objective Function. *Journal of the*
863 *American Statistical Association*, 58(301).
864 <https://doi.org/10.1080/01621459.1963.10500845>
- 865 Worbe, Y., Baup, N., Grabli, D., Chaigneau, M., Mounayar, S., McCairn, K., Feger, J., &
866 Tremblay, L. (2009). Behavioral and movement disorders induced by local inhibitory
867 dysfunction in primate striatum. *Cereb Cortex*, 19(8), 1844-1856.
868 <https://doi.org/10.1093/cercor/bhn214>
- 869 Xue, J., Qian, D., Zhang, B., Yang, J., Li, W., Bao, Y., Qiu, S., Fu, Y., Wang, S., Yuan, T.
870 F., & Lu, W. (2022). Midbrain dopamine neurons arbiter OCD-like behavior. *Proc*
871 *Natl Acad Sci U S A*, 119(46), e2207545119.
872 <https://doi.org/10.1073/pnas.2207545119>

873 Zhang, Y. F., Vargas Cifuentes, L., Wright, K. N., Bhattarai, J. P., Mohrhardt, J., Fleck, D.,
874 Janke, E., Jiang, C., Cranfill, S. L., Goldstein, N., Schreck, M., Moberly, A. H., Yu,
875 Y., Arenkiel, B. R., Betley, J. N., Luo, W., Stegmaier, J., Wesson, D. W., Spehr, M.,
876 . . . Ma, M. (2021). Ventral striatal islands of Calleja neurons control grooming in
877 mice. *Nat Neurosci*, 24(12), 1699-1710. <https://doi.org/10.1038/s41593-021-00952->
878 z

879

JNeurosci Accepted Manuscript

880 **Figure legends**881 **Figure 1. Experimental procedures.**

882 **(A)** Localization of injection sites using computed tomography (CT) and magnetic
883 resonance (MR) imaging. Left: CT image visualizing the injection cannulae targeting the
884 bilateral VS (hot color) overlaid on the MR image (grayscale) from monkey RI. Right:
885 muscimol injection sites, with each purple circle representing an estimated muscimol
886 diffusion area (~3 mm) from the tip of cannula marked on an MR image from monkey BI.
887 Dotted lines indicate VS boundaries within the striatum. “AC+” indicates the anterior
888 distance from the center of the anterior commissure. **(B)** Illustration of the test cage
889 environment for free-moving behavior. During the session, each monkey was isolated
890 within the cage for observation and recording. **(C)** Reward-size task sequence. Left: trial
891 sequence. Each trial began when the monkey gripped a bar mounted at the front of the
892 chair. If the monkey continued to grip, a black-and-white image (‘cue’) and a colored square
893 appeared on the screen. Upon the appearance of a green square (‘go’ signal), the monkey
894 was required to release the bar within 200–1000 ms to receive a liquid reward. If the
895 monkey released the bar before the ‘go’ signal or held the bar for longer than 1 s, the trial
896 was marked as an error, and no water reward was provided. A correct release turned the
897 screen spot blue (‘correct’ signal). Right: reward contingency. A reward of 1, 2, 4, or 8
898 drops of water (1 drop = approximately 0.12 mL) was delivered immediately after the
899 correct signal. Each reward size was selected randomly with equal probability, and the cue
900 presented at the beginning of the trial indicated the reward amount for that trial.

901

902 **Figure 2. Ventral striatum (VS) inactivation induced location-specific behaviors in the**
 903 **cage.**

904 **(A)** Representative behaviors were observed in the cage during the muscimol injection
 905 sessions. Top: “resting” behavior, characterized by the monkeys sitting with their head
 906 down and remaining motionless without lying down. Bottom: “checking” behavior, in which
 907 the monkeys repetitively pinched at the corners of the cage from various angles, frequently
 908 changing the pattern and posture of checking. The histograms illustrate examples of the
 909 “resting” (mus-B6 and mus-R5 in Table S1) and “checking” behaviors (mus-B2 and mus-
 910 R2) during the sessions of both monkeys. The horizontal axis represents time, and the
 911 vertical axis denotes the number of frames showing each behavior (orange: “standing,”
 912 purple: “resting,” blue: “grooming,” green: “biting,” red: “checking”.) **(B)** Proportional
 913 distributions of the five observed behaviors across sessions. The muscimol injection
 914 sessions (top) are arranged from the anterior to posterior VS injection sites. The horizontal
 915 axis shows the proportions of each behavior, whereas the vertical axis represents the
 916 session ID. **(C)** Hierarchical clustering dendrogram (Ward’s method with Euclidean
 917 distance) of sessions based on behavioral profiles. The vertical axis shows the clustering
 918 distance, whereas the horizontal axis displays the session IDs (mus: muscimol injection
 919 session, con: control session; B: monkey BI, R: monkey RI; numbers indicate the session
 920 ID for each treatment; for example, “mus-B1” represents the first muscimol injection
 921 session for monkey BI). The pie charts illustrate the mean behavior proportions within each
 922 cluster. **(D)** Injection site mapping on magnetic resonance images from the two monkeys,
 923 aligned along the anterior–posterior axis of the VS with the anterior tip at VS +0. Each circle
 924 marks an injection site (estimated muscimol diffusion area), with the color indicating the
 925 cluster destination (cyan = cluster 1, magenta = cluster 5). Dotted lines indicate VS
 926 boundaries within the striatum. The muscimol diffusion remained within the VS in 18 of 26
 927 injections. Cluster 1 corresponds to the anterior VS (aVS) and cluster 5 corresponds to the
 928 posterior VS (pVS), based on the distinct localization patterns along the VS.

929

930 **Figure 3. Effects of local ventral striatum (VS) inactivation in the reward-size task.**

931 **(A)** Cumulative error counts over time for each treatment in the reward-size task. Data for
932 monkey BI (left) and monkey RI (right) are shown as the mean \pm standard error of the
933 mean, with different treatments indicated by color: the anterior VS (aVS) in blue, the
934 posterior VS (pVS) in red, and the control in gray. Asterisks denote significant differences
935 between treatments ($*p < 0.05$, one-way analysis of variance with post-hoc Tukey's
936 honestly significant difference test). **(B)** Cumulative reward earning over time across
937 treatments (mean \pm standard error of the mean). **(C)** Total number of trials initiated under
938 each treatment condition. **(D)** Early error rates for each treatment condition. Center lines
939 indicate means, box limits represent the first and third quartiles, and whiskers extend from
940 minimum to maximum values. **(E)** Injection sites (estimated muscimol diffusion area) are
941 plotted on magnetic resonance images, with each site represented by a colored circle.
942 Dotted lines indicate VS boundaries within the striatum. In 33 of 52 injections, the muscimol
943 diffusion remained within the VS. The color gradient from blue to red indicates the
944 normalized error rate per session, with values from 0 (blue) to 1 (red).

945

946 **Figure 4. Changes in goal-directed behaviors during the early and late phases of the**
947 **task.**

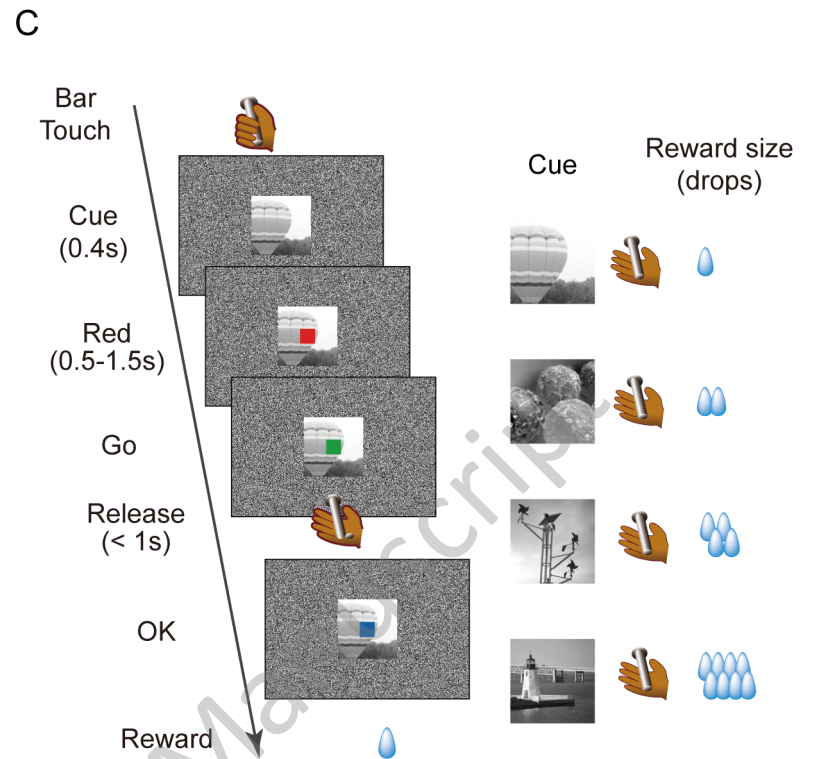
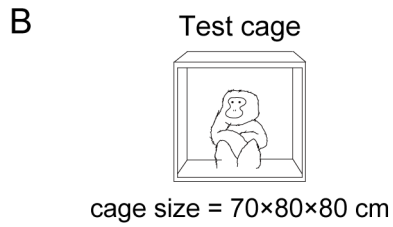
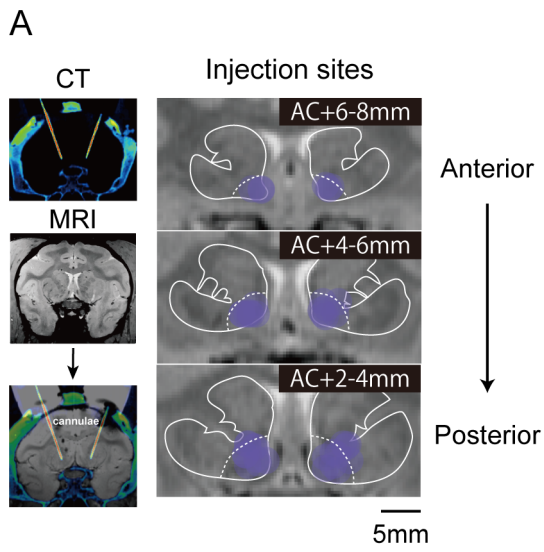
948 Top row (A–D): Injection sites for each inactivation condition are displayed on anatomical
949 images. Bottom row (A–D): Error rates for each reward size (1, 2, 4, and 8 drops) during
950 the first (left) and last (right) 25 min of the task. The results for each inactivation condition
951 are shown below. **(A)** Anterior ventral striatum (aVS), in blue. **(B)** Posterior ventral striatum
952 (pVS), in red. **(C)** Rostromedial caudate (rmCD), in cyan. **(D)** Ventral pallidum (VP) is
953 yellow. Control sessions are shown in black. Each dot represents the mean error rate, with
954 error bars indicating the standard error of the mean. Dotted curves represent the best-fit
955 inverse function for each condition. Asterisks indicate significant main effects or interaction
956 ($*p < 0.05$, two-way analysis of variance with post-hoc Tukey's honestly significant
957 difference test). AC: anterior commissure, Cd: caudate, GPe: external segment of globus
958 pallidus, Put: putamen, VP: ventral pallidum.

959 **Figure 5. Anatomical projection patterns to the anterior ventral striatum (aVS) and**
960 **posterior ventral striatum (pVS).**

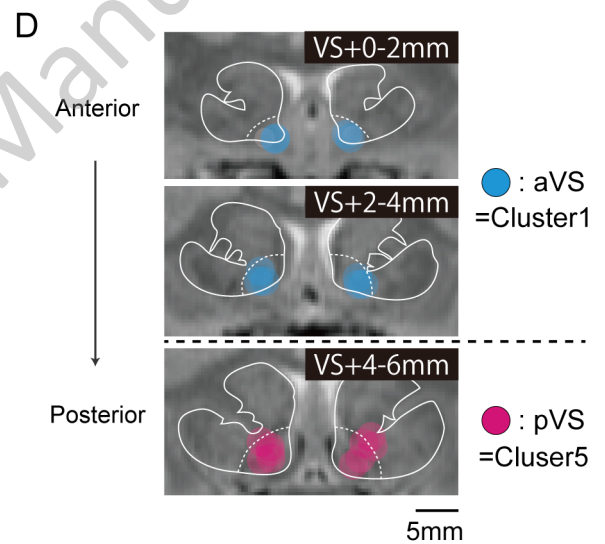
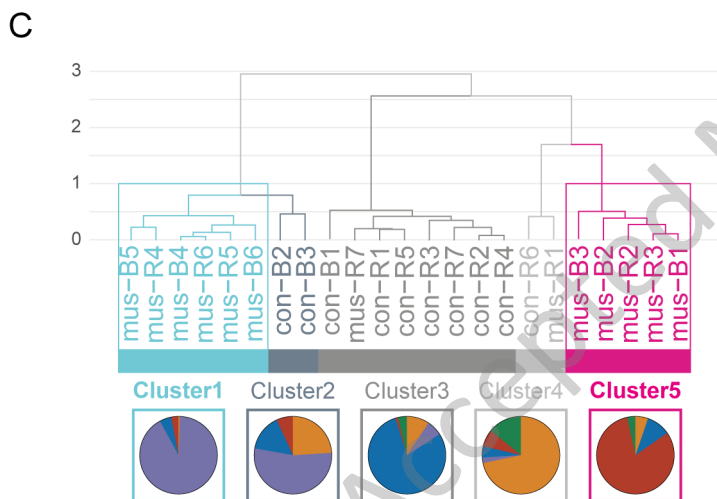
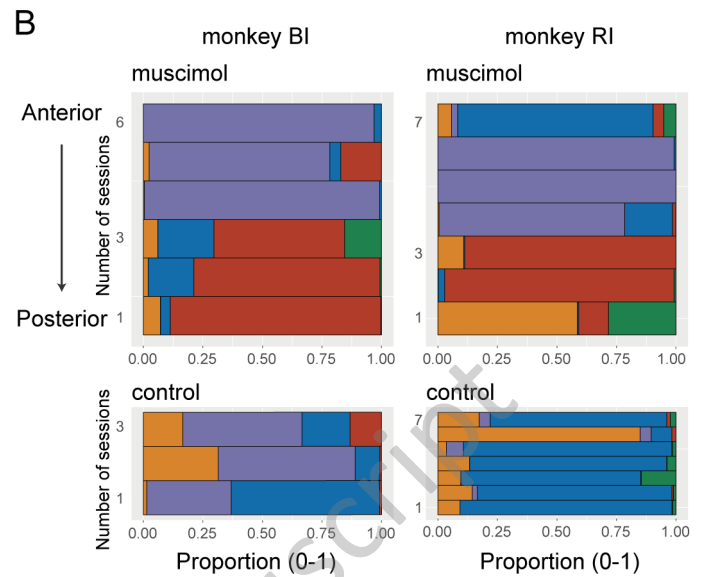
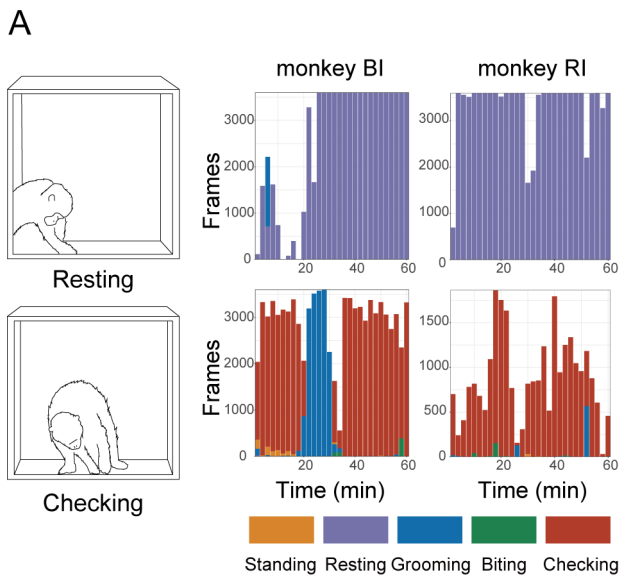
961 **(A)** Schematic illustration of the injection sites of retrograde viral vectors in the aVS and
962 pVS (left) alongside a fluorescently stained image (right). In a single monkey (monkey
963 #250), AAV2retro-hSyn-mScarlet was injected into the aVS of the left hemisphere, and
964 AAV2retro-hSyn-AcGFP was injected into the pVS of the right hemisphere. **(B)** Coronal
965 sections showing mScarlet and green fluorescent protein (GFP) expression along a rostral
966 to caudal gradient, with sections labeled 1 to 4. These panels represent sections at
967 different anterior–posterior coordinates. (1: AC +18.45 mm, 2: AC +16.2 mm, 3: AC +14.4
968 mm, and 4: AC +0.45 mm). Regions expressing mScarlet and GFP are shaded in red and
969 green, respectively, with the color intensity qualitatively indicating expression strength. The
970 text colors correspond to mScarlet (red) and GFP (green) expression; black text denotes
971 regions expressing both markers. The fluorescently stained image in the upper right
972 corresponds to schematic 1 (scale bar = 2 mm), and the inset shows an example of
973 retrogradely labeled neurons expressing the fluorescent proteins (scale bar = 100 μ m).
974 ACC: anterior cingulate cortex, AIC: anterior insular cortex, Amy: amygdala, ABpc:
975 accessory basal nucleus of the amygdala, parvicellular division, Bi: basal nucleus of the
976 amygdala, intermediate subdivision, Bpc: basal nucleus of the amygdala, parvicellular
977 subdivision, dmPFC: dorsomedial prefrontal cortex, EC: entorhinal cortex, IOFC: lateral
978 orbitofrontal cortex, TC: temporal cortex, vmPFC: ventromedial prefrontal cortex.

979

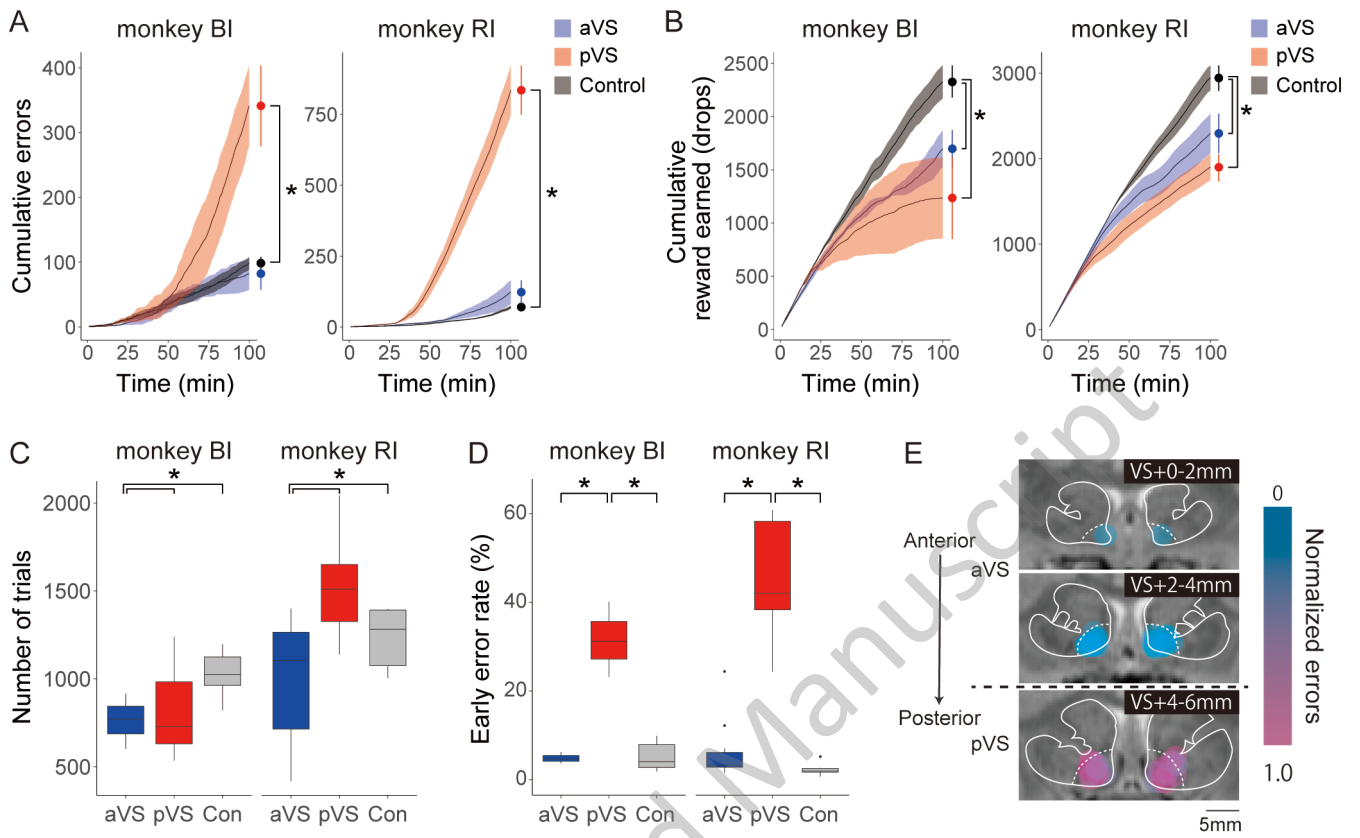
980



JNeurosci Accepted Manuscript



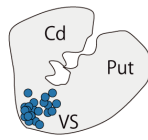
JNeurosci Accepted Manuscript



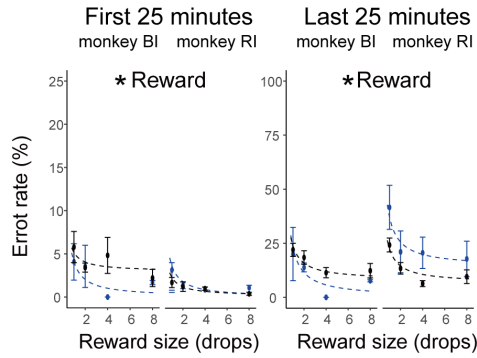
JNeurosci Accepted Manuscript

A

aVS

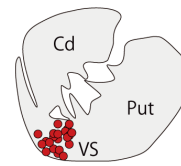


AC+4~8mm

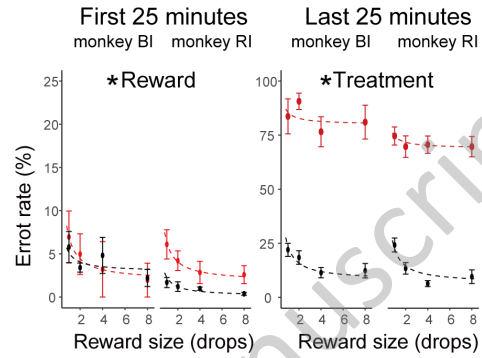


B

pVS

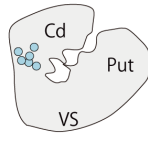


AC+2~4mm

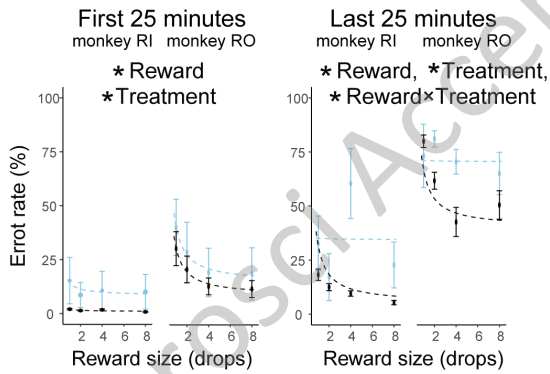


C

rmCD

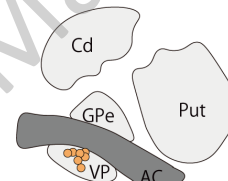


AC+4~8mm



D

VP



AC-2~0mm

